



Article

Calibration Inter-Comparison of MODIS and VIIRS Reflective Solar Bands Using Lunar Observations

Xiaoxiong Xiong ¹, Junqiang Sun ² , Amit Angal ^{2,*} and Truman Wilson ²¹ Sciences and Exploration Directorate, NASA Goddard Space Flight Center, Greenbelt, MD 20771, USA² Science Systems and Applications Inc., 10210 Greenbelt Road, Lanham, MD 20706, USA

* Correspondence: amit.angal@ssaihq.com

Abstract: Multispectral band observations from Terra and Aqua MODIS, launched in December 1999 and May 2002, respectively, and from SNPP and NOAA-20 VIIRS, launched in November 2011 and October 2017, respectively, have continuously enabled a broad range of applications and studies of the Earth system and its changes via a set of geophysical and environmental parameters. The quality of MODIS and VIIRS science and environmental data products relies strongly on the calibration accuracy and stability of individual sensors, as well as their calibration consistency, especially for the data products generated using observations from sensors across different platforms. Both MODIS and VIIRS instruments carry a similar set of on-board calibrators for their on-orbit calibration. Besides, lunar observations are regularly scheduled and implemented in support of their reflective solar bands (RSB) calibration, especially their long-term stability monitoring. In this paper, we provide an overview of MODIS and VIIRS solar and lunar calibration methodologies applied for the RSB on-orbit calibration, and describe the approach developed for their calibration inter-comparisons using lunar observations, including corrections for the effects caused by differences in the relative spectral response and adopted solar spectra between individual sensors. The MODIS and VIIRS calibration inter-comparison results derived from their regularly scheduled lunar observations are presented and discussed, including associated uncertainties and a comparison with those derived using the Earth-view targets. Also discussed are remaining challenges in lunar calibration and inter-comparison for the Earth-observing sensors, as well as on-going efforts for future improvements.

Keywords: MODIS; VIIRS; solar calibration; lunar calibration; calibration inter-comparison; moon



Citation: Xiong, X.; Sun, J.; Angal, A.; Wilson, T. Calibration Inter-Comparison of MODIS and VIIRS Reflective Solar Bands Using Lunar Observations. *Remote Sens.* **2022**, *14*, 4754. <https://doi.org/10.3390/rs14194754>

Academic Editors: Raad A. Saleh and Zhuosen Wang

Received: 28 July 2022

Accepted: 19 September 2022

Published: 23 September 2022

Publisher's Note: MDPI stays neutral with regard to jurisdictional claims in published maps and institutional affiliations.



Copyright: © 2022 by the authors. Licensee MDPI, Basel, Switzerland. This article is an open access article distributed under the terms and conditions of the Creative Commons Attribution (CC BY) license (<https://creativecommons.org/licenses/by/4.0/>).

1. Introduction

Since their launches on 18 December 1999, and 4 May 2002, NASA's Terra and Aqua Moderate Resolution Imaging Spectroradiometer (MODIS) instruments have successfully operated for more than 22 and 20 years, respectively. MODIS observations, made in 36 spectral bands covering wavelengths from visible (VIS) to long-wave infrared (LWIR), have generated numerous data products that have significantly contributed to the remote sensing community and users worldwide for numerous advanced studies of the Earth's system and its key geophysical and environmental parameters, as well as their changes over various temporal scales and geographic regions [1–9]. Developed by the same instrument vendor, the Visible Infrared Imaging Radiometer Suite (VIIRS) is a MODIS follow-on sensor designed to further extend and improve the global observations made by the MODIS instruments as well as many of their environmental products that have been widely used for comprehensive studies of the Earth's system of land, oceans, and atmosphere [10–18]. To date, two VIIRS instruments have successfully operated onboard the Suomi National Polar-Orbiting Partnership (SNPP) and NOAA-20 (N20) satellites for more than 10 and 4 years since their respective launches on 28 October 2011 and 18 November 2017. As expected, the scientific value and significance of MODIS and VIIRS observations and their associated applications will continue to increase with time, especially with future launches

of three identical VIIRS instruments onboard the Joint Polar Satellite System (JPSS) satellites, JPSS-2, -3, and -4 within the next ten years. This could potentially allow the current data records to extend beyond four decades [17,18]. JPSS-2 VIIRS is scheduled to launch in November 2022 and has recently completed its spacecraft-level integration and testing in the thermal vacuum environment.

The quality of MODIS and VIIRS data products depends strongly on their on-orbit calibration accuracy and stability, and their calibration consistency, especially for products and applications developed using observations from sensors operated on different satellites or platforms [14–16,19–23]. Both MODIS and VIIRS instruments, designed and built by Raytheon Santa Barbara Remote Sensing (SBRS, located in Goleta, CA, USA) and now Raytheon Intelligence & Space (RIS, located in El Segundo, CA, USA), carry a similar set of on-board calibrators (OBC) that include a solar diffuser (SD), a solar diffuser stability monitor (SDSM), a blackbody (BB), and a space view (SV) port. MODIS has an additional device, called the Spectroradiometric Calibration Assembly (SRCA) that was not included in VIIRS. The SD/SDSM system is used primarily for the reflective solar bands (RSB) calibration and the BB for the thermal emissive bands (TEB) calibration. The dedicated SV port provides measurements of instrument background, including thermal background and detector or electronic offsets, on a scan-by-scan basis [10,24–26]. Twenty of the thirty-six MODIS spectral bands (bands 1–19 and 26) are the RSB, covering wavelengths from 0.41 to 2.4 μm and at nadir spatial resolutions of 250 m for bands 1–2, 500 m for bands 3–7, and 1 km for the remaining bands. VIIRS has 14 RSB (M1–M11 and I1–I3) that cover nearly the same wavelength range as MODIS. Its imagery bands (I bands) have a nadir spatial resolution of 375 m while the moderate resolution bands (M bands) have a nadir spatial resolution of 750 m. Several VIIRS bands can make measurements at either high or low gain, thus referred to as the dual gain bands. Table 1 is a summary and side-by-side comparison of the MODIS and VIIRS RSB spectral wavelengths and their horizontal spatial resolutions (HSR). The VIIRS day and night band (DNB) is comprised of three gain stages covering a wavelength range from 0.5 to 0.9 μm and is greatly impacted by the on-orbit change in the relative spectral response (RSR) in SNPP. A study of the intercomparison results using lunar data was conducted in previous work, and therefore it is not included in this study [27].

Table 1. Spectral wavelengths and spatial resolutions at the nadir of MODIS and VIIRS reflective solar bands (RSB).

VIIRS Band	Spectral Range (μm)	HSR (m)	MODIS Band	Spectral Range (μm)	HSR (m)
DNB	0.500–0.900				
M1	0.402–0.422	750	8	0.405–0.420	1000
M2	0.436–0.454	750	9	0.438–0.448	1000
M3	0.478–0.498	750	3 10	0.459–0.479 0.483–0.493	500 1000
M4	0.545–0.565	750	4 12	0.545–0.565 0.546–0.556	500 1000
I1	0.600–0.680	375	1	0.620–0.670	250
M5	0.662–0.682	750	13 14	0.662–0.672 0.673–0.683	1000 1000
M6	0.739–0.754	750	15	0.743–0.753	1000
I2	0.846–0.885	375	2	0.841–0.876	250
M7	0.846–0.885	750	16 2	0.862–0.877 0.841–0.876	1000 250
M8	1.230–1.250	750	5	SAME	500

Table 1. Cont.

VIIRS Band	Spectral Range (μm)	HSR (m)	MODIS Band	Spectral Range (μm)	HSR (m)
M9	1.371–1.386	750	26	1.360–1.390	1000
I3	1.580–1.640	375	6	1.628–1.652	500
M10	1.580–1.640	750	6	1.628–1.652	500
M11	2.225–2.275	750	7	2.105–2.155	500

In addition to SD/SDSM measurements, lunar observations are scheduled on a near-monthly basis and used in support of MODIS and VIIRS RSB on-orbit calibration stability monitoring [28–30]. The Moon provides an extremely stable radiometric calibration reference, especially in the reflective solar spectral regions. A lunar model, known as the Robotic Lunar Observatory (ROLO) model, developed at the USGS, is used to provide the predicted lunar irradiances (integrated over the entire lunar surface) for Earth-observing sensors [31–33]. Similar to MODIS and VIIRS, many Earth-observing sensors monitor their on-orbit calibration stability with comparisons of their calibrated lunar responses with the predicted lunar irradiances from the ROLO model [34–38]. The MODIS and VIIRS instruments view the Moon regularly through their SV ports, often coupled with spacecraft roll maneuvers. These spacecraft maneuvers are also coupled with a data sector rotation, where the wide field-of-view (FOV) Earth-view (EV) data sector is rotated such that it covers the SV port (the SV data sector FOV is narrow compared to the actual port size). Each instrument has its lunar observations kept within a small phase angle range, typically within 1 degree of its selected phase angle. The roll maneuvers are restricted to a narrow range (0 to -20° for MODIS, and 0 to -14° for VIIRS) to prevent unwanted radiation from Earth impinging on the radiative cooler. As of 1 July 2022, the Terra and Aqua MODIS instruments have scheduled and performed 216 and 205 lunar observations with most of their phase angles near $+55^\circ$ and -55° , respectively. The SNPP and N20 VIIRS, operated in the same orbit approximately 50 min apart, have made 90 and 39 lunar observations, respectively, with their phase angles mostly centered at -51.5° . The plus (+) phase angle refers to viewing a waning Moon whereas the minus (−) sign corresponds to a waxing Moon.

Apart from supporting the RSB on-orbit calibration and stability monitoring, lunar observations can be also used to assess the TEB calibration stability, the sensor spatial characterization performance, and cross-sensor calibration inter-comparisons [39–43]. This paper focuses on calibration inter-comparisons of MODIS and VIIRS RSB using their regularly scheduled lunar observations. It includes assessments and corrections applied to account for the effects due to the individual sensors' RSR and their adopted solar spectra. For MODIS, this study will not include its short-wave infrared (SWIR) bands that have different levels of thermal leak and electronic crosstalk, which are known issues identified since pre-launch testing [44]. Although a correction algorithm applied to the Level 1B (L1B) for the EV observations has been effective in general, its application to the lunar observations, which have much higher thermal infrared signals, presents additional challenges in order to achieve results of the same level of radiometric accuracy as other RSB for high quality cross-sensor calibration inter-comparisons.

In the following, we provide a brief overview of MODIS and VIIRS solar and lunar calibration methodologies in Section 2, along with their applications for the RSB on-orbit calibration. The approaches of using lunar observations for MODIS and VIIRS RSB calibration inter-comparison are presented in Section 3, as well as the adjustments or corrections applied to address the impact due to sensor-specific RSR and selected solar spectra. Section 4 presents the results of this study, including examples of the lunar irradiance trending based on sensor measurements and that from the ROLO model predictions, and the calibration differences between the two MODIS, two VIIRS, and MODIS and VIIRS instruments. Also discussed in Section 4 are key uncertainty contributors involved in the lunar calibration inter-comparison process, as well as a comparison of calibration differences derived from

lunar observations with that from the observations of EV targets. Section 5 is a short summary of this study. As illustrated in this paper, both MODIS and VIIRS RSB have been well calibrated using their on-board solar diffusers and lunar observations, allowing high quality data products to be generated over their entire missions. The calibration differences between the Terra and Aqua MODIS VIS/NIR bands are generally small, within their combined uncertainties. For the two VIIRS instruments, however, several band pairs have shown large calibration differences of up to 3.8% that are likely due to larger than expected pre-launch calibration uncertainties associated with their solar diffuser calibration system. Results of this study will greatly help the science community and algorithm developers with a better understanding of MODIS and VIIRS calibration quality and calibration biases in the current data products and support their efforts, including strategies to address sensor differences, to generate high-quality climate data records using observations from multiple sensors. The approaches and techniques presented in this paper will also benefit other Earth-observing instruments that either have acquired or plan to acquiring on-orbit lunar observations for their calibration stability monitoring and calibration inter-comparisons with other instruments and for the generation of consistent environmental data products.

2. MODIS and VIIRS Solar and Lunar Calibration

In this section, the MODIS and VIIRS RSB solar and lunar calibration algorithms and results applied in support of their L1B production are presented with the main focus on their calibration similarities and differences. For both Terra and Aqua MODIS, the current L1B in production is Collection 6.1 (C6.1). Recently, the MODIS Characterization Support Team (MCST) completed and delivered its latest Collection 7 (C7) algorithms and corresponding calibration look-up tables (LUTs) in support of a new mission reprocess of all MODIS data products. C7 L1B reprocessing is expected to start in late 2022. In this paper, the MODIS SD and lunar calibration algorithms and results are based on this new L1B collection. The latest NASA VIIRS L1B collection is C2 for SNPP and C2.1 for N20. More details of the latest MODIS and VIIRS calibration algorithms can be found in a number of references [45–47]. To a large extent, the VIIRS RSB calibration methodologies and strategies were inherited and improved based on lessons from the MODIS calibrations and operations. A few key differences do exist due to instrument design specifics and algorithm enhancements. In the following, the MODIS RSB SD and lunar calibration algorithms and applications are reviewed first and this is followed by a similar discussion for VIIRS.

2.1. MODIS

For both MODIS instruments, a linear relationship or algorithm between the incident radiance (L) and detector response (dn^*) is applied for the RSB calibration and retrieval,

$$L = \frac{m_1 E_{Sun} dn^*}{\pi RVS}, \quad (1)$$

where m_1 is the calibration coefficient (inversely proportional to the gain of a given detector) derived with reference to the SD bi-directional reflectance factor (BRF), E_{sun} is the solar spectral irradiance at an Earth–Sun distance of 1 astronomical unit (AU) and integrated over the RSR for each detector, dn^* is the detector digital response corrected for instrument background and temperature effects, and RVS is the response versus scan angle, which accounts for the instrument gain variations as a function of the angle of incidence (AOI) of light relative to the scan mirror. Since the SD is used primarily for MODIS RSB calibration, the RSB RVS is conveniently normalized at the AOI of its SD view, i.e., $RVS_{SD} = 1$. For the EV observations, the MODIS RSB L1B primary data product is the top-of-atmosphere (TOA) reflectance factor, $\rho_{EV} \cos(\theta_{EV})$, where θ_{EV} is the solar zenith angle of the EV pixel. The EV radiance, L_{EV} , and the reflectance factor, $\rho_{EV} \cos(\theta_{EV})$, can be easily converted to each other by multiplying or dividing a factor of $\frac{E_{Sun}}{\pi d_{ES}^2}$, with d_{ES} being the Earth–Sun distance (normalized at 1 AU) at the time of sensor observation. The solar spectral irradiance used in the MODIS RSB is a combination of Thuillier et al. (1998; 0.4–0.8 μm), Neckel and Labs

(1994; 0.8–1.1 μm), and Smith and Gottlieb (above 1.1 μm) [9]. MODIS L1B calibration algorithms produce both radiance and reflectance data products for the RSB.

The on-orbit calibration coefficient m_1 and RVS in Equation (1) change with time and are thus updated regularly. For both MODIS instruments, the m_1 and the RVS are currently derived by using the SD calibration, lunar calibration, and EV observations over select desert sites at multiple AOIs.

The MODIS SD is a flat and near-rectangular panel made of Spectralon with a near-Lambertian reflectance profile. It is located inside the instrument cavity. The SD provides diffusely reflected sunlight that can be used for the RSB calibration. The SD panel can be illuminated by the sun when the instrument passes the Earth terminator from the nighttime side to the daytime side. Only the responses to the fully illuminated SD are used to compute the calibration coefficients. Figure 1a shows a schematic of the MODIS scan operation that enables data to be collected each scan from its on-board calibrators and the EV. The left side of Figure 1b shows the AOI of each of the OBC in relation to the EV data. During each SD calibration, the solar radiance diffusely reflected from the SD can be accurately calculated by

$$L_{SD} = \frac{\rho_{SD} \cos(\theta_{SD}) \Delta_{SD} \tau_{SDS} E_{Sun}}{\pi d_{ES}^2}, \quad (2)$$

where ρ_{SD} is the SD BRF derived from prelaunch measurements, θ_{SD} is the solar zenith angle relative to the SD, Δ_{SD} is the SD on-orbit degradation, and τ_{SDS} is the SD screen (SDS) transmission function, which is also referred to as the vignetting function (VF). During sensor nominal operations, the SDS can be commanded to an open or a closed position, thus providing two different levels of the intensity for the sunlight illuminated on the SD surface. Placed in front of the SDS is an aperture door that is only opened during nominally scheduled SD and SDSM calibration events. For Terra MODIS, however, the SD door has been fixed in the open position with the SDS in the closed position since 2 July 2003, resulting from an anomaly related to its SD door and/or SDS operation. The SD BRF was measured prelaunch, and its relative profile was validated on-orbit using measurements made during spacecraft yaw maneuvers, which were performed early in the mission for both Terra and Aqua MODIS. The SD on-orbit degradation, Δ_{SD} , is tracked by the onboard SDSM. For MODIS, the SDS VF was not fully characterized prelaunch, and it was derived on-orbit from measurements during yaw maneuvers made with and without the SDS in place. When the SDS is placed in the open position during an SD calibration event, τ_{SDS} in Equation (2) becomes a constant of 1. Otherwise, it varies with the solar illumination angle relative to the SDS. In Equation (2), an assumption that the SD degrades uniformly with respect to incident and outgoing directions has been applied, meaning that the degradation measured at the output angle of the SDSM will be the same as in the direction of the RSBs. Therefore, the SD on-orbit BRF can be expressed as the product of its prelaunch BRF, ρ_{SD} , and its on-orbit degradation, Δ_{SD} [47]. However, evidence of non-uniformity in the SD degradation has led to the use of EV data to supplement the calibration of the MODIS RSB, which will be discussed further below.

By applying Equation (1) to the SD view and substituting L_{SD} in Equation (2) to Equation (1), we can derive the calibration coefficient by

$$m_1 = \frac{\rho_{SD} \cos(\theta_{SD}) \tau_{SDS} \Delta_{SD}}{dn_{SD}^* d_{ES}^2}, \quad (3)$$

The calibration coefficient is calculated for each band, detector, and mirror side for the 1-km RSB as well as for each sub-frame for the 500-m (2) and 250-m (4) resolution RSBs.

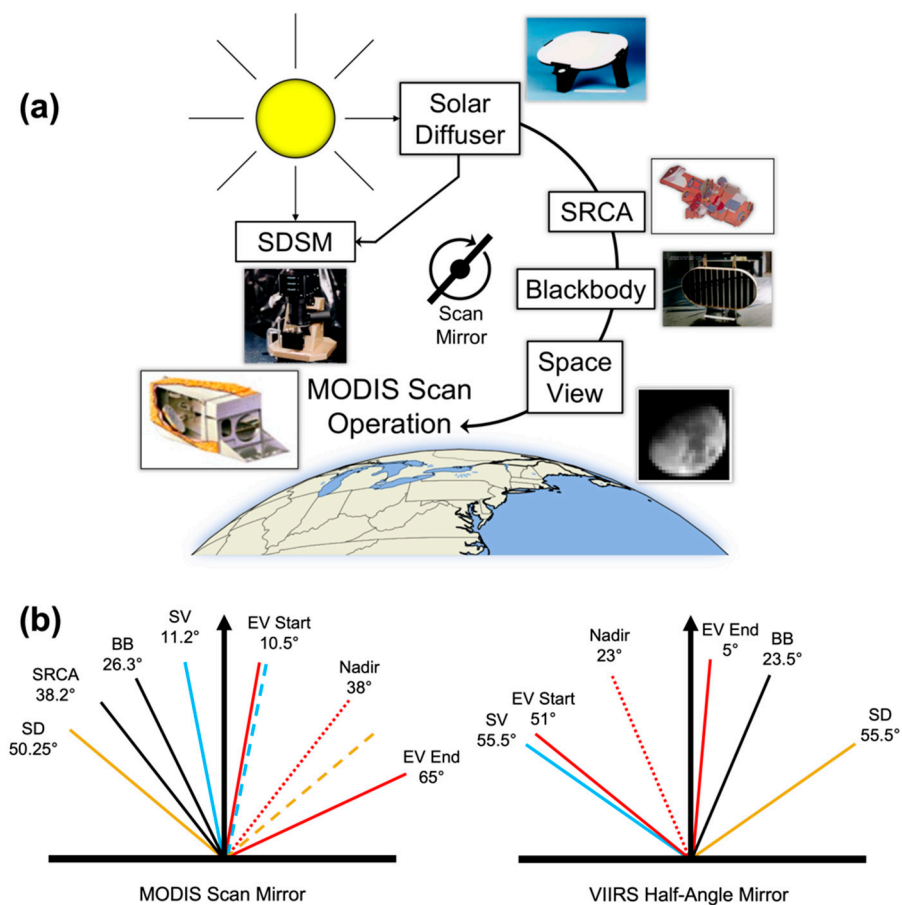


Figure 1. (a) Schematic of MODIS scan operation and instrument OBCs. The VIIRS instrument has a similar configuration. (b) AOI on the scan mirror (MODIS, left) and half-angle mirror (VIIRS, right) for the OBCs and the EV. The dashed lines show the projection of the MODIS AOI onto the EV AOI when computing the RVS.

As previously mentioned, the SD on-orbit degradation, Δ_{SD} , in Equation (3) is tracked by the SDSM, which functions as a ratioing radiometer that views the SD, the Sun through its Sun-view port, and an internal dark scene, alternately. The MODIS SDSM has nine detectors, and each detector tracks the SD degradation at a discrete wavelength. The center wavelengths of the SDSM detectors cover a spectral range from 412 nm to 936 nm. After corrections applied for the view geometry effects, the ratios of the background subtracted digital count for the SD view to the background subtracted digital count of the Sun view provide the trends of the SD on-orbit degradation. The response of the SDSM detectors is assumed to be linear. It was also assumed that the SD degradation between its prelaunch characterization and its first on-orbit measurement was negligible since the SD exposure to the environment was minimal. Consequently, the SDSM ratios normalized to its first on-orbit SD measurements are used to track the SD on-orbit degradation at the wavelengths of its detectors. A linear interpolation approach is applied to obtain the SD degradation at any wavelength in the range from 0.412 μm to 0.936 μm from the measured SD degradations at the nine center wavelengths of the SDSM detectors [48,49].

The lunar surface has a long history of use as a calibration target for the reflective bands of a number of satellite instruments, owing to its stable reflective surface and lack of atmosphere [50]. Since the lunar surface is not smooth, only the integrated lunar irradiance is used in the MODIS lunar calibration methodology. Using Equation (1), the measured

lunar radiance from individual detectors can be easily calculated and their corresponding integrated lunar irradiance (I) can be expressed by

$$I = \frac{1}{N} \sum \frac{m_1 E_{Sun} dn_{Moon}^*}{\pi RVS} \omega, \quad (4)$$

where N is number of the scans used in the computation, each of which fully covers the lunar surface, and $\omega = 1/(705S_{tot})^2$ is the solid angle (steradians) of each pixel. S_{tot} is the number of sub-frames of each band (or detector) and 705 km is the nominal orbital altitude. The value of $1/S_{tot}$ corresponds to the HSR at the nadir in km. The summation is made over detectors, frames, and select scans. In this analysis, the lunar irradiance is calculated using the MODIS C7 LUTs prepared for the upcoming L1B reprocessing. Instead of using only scans that fully cover the lunar surface, the lunar irradiance can also be calculated using the measurements from all scans in a lunar observation event. Using all scans requires the creation of lunar images corresponding to each detector in order to be able to use images where the Moon is only partially on the FPA. These detector images are created by extracting single lines from each scan corresponding to the detector as the Moon moves across the FPA. This approach, however, requires a correction for the oversampling effects. Oversampling occurs because the Moon does not move on the FPA by 1 pixel per scan, causing some parts of the lunar surface to be observed more than once in a detector image (higher resolution bands can be undersampled under certain observation geometries). The all-scan approach has a relatively large uncertainty due to corrections applied for the oversampling effect, but it can help examine calibration differences among individual detectors. In this analysis we focus on the methodology that uses the scans with full coverage of the lunar surface as described by Equation (4). Figure 2a,b show examples of the lunar images acquired by Aqua MODIS bands 1 and 8 during the scheduled lunar observation on 24 January 2021. Also shown in Figure 2 are the lunar images acquired by the SNPP VIIRS on the same day for its bands I1 (c) and M1 (d).

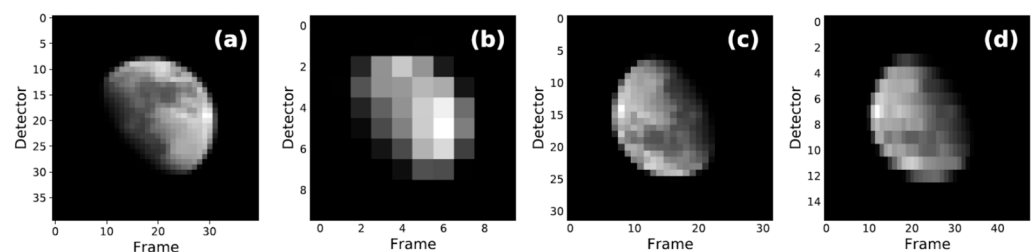


Figure 2. Lunar images acquired on 24 January 2021. (a) Aqua MODIS band 1. (b) Aqua MODIS band 8. (c) SNPP VIIRS band I1. (d) SNPP VIIRS band M1. In (d), the pixel aspect ratio was set to 3:1 in order to produce a circular Moon image.

By comparing the integrated lunar irradiance predicted by the ROLO model (I^{ROLO}) with that measured by the MODIS using Equation (4), the band-averaged calibration coefficient, m_1^{Moon} , can be computed by

$$m_1^{Moon} = \frac{N\pi RVS I^{ROLO} \langle m_{1,0} \rangle}{\sum m_{1,0} E_{Sun} dn_{Moon}^* \omega} \quad (5)$$

where $m_{1,0}$ are the calibration coefficients derived from the first SD on-orbit calibration and the angled brackets indicate an average over all detectors of the band. To calibrate the RSB using the Moon, a reference for the lunar irradiance is required. In this analysis, the lunar irradiance for each calibration in Equation (5) was provided by the Robotic Lunar Observatory (ROLO) model prediction, developed by the USGS [31]. Since the absolute uncertainty of the current ROLO lunar model is larger than the MODIS calibration specification of 2%, the MODIS lunar calibration is only used to track the RSB on-orbit

changes. In this case, the constant terms in Equation (5) can be omitted in routine data processing [28].

Among the RSBs, bands 13–16 partially saturate when they observe the Moon. This saturation occurs at the inner part of the illuminated lunar surface (with unsaturated pixels near the disk edge and terminator), which is typically at the highest radiance levels. To correct for saturation, a ratio approach is applied to replace the saturated pixels using band 18 as a reference band [51]. To obtain the ratio, the saturated band data is plotted versus the spatially co-registered reference band data at the pixel level and fit to a linear equation for all unsaturated pixels, where the slope represents the ratio between the two bands. The saturated data can then be replaced by multiplying the reference band data by the ratio at the location of the saturated pixels. For SWIR bands, there are strong crosstalk contaminations among themselves and from mid-wave infrared bands as well as the large out-of-band (OOB) RSR contributions at the wavelength of 5.3 μm . These contaminations need to be mitigated before the calculation of the lunar irradiance using Equation (4). Accurate mitigation of these effects is still a challenging issue and needs more effort [52]. In this analysis, MODIS lunar calibration is mainly focused on the VIS and NIR bands.

For MODIS RSBs, the calibration coefficients, m_1 , and the RVS are needed to produce the L1B products as shown in Equation (1). Due to the non-uniformity of the SD degradation with respect to the incident and outgoing directions, the SD degradation measured at the SDSM view direction may deviate from that at the RSB view direction, resulting in a long-term bias in the calibration coefficients derived from the SD, especially for short wavelength RSB that have experienced more significant degradation on-orbit. As a result, EV response trends from pseudo-invariant desert sites at the SD AOI are used to correct the long-term drifts in SD-based calibration coefficients for the short wavelength bands. Combination of the SD calibration results and EV response trends at the same AOI help produce the calibration coefficients with both long-term accuracy and short-term stability [53].

MODIS RSBs view the SV, through which the Moon is also observed, and the SD at different AOIs to the scan mirror, with the SV at 11.25° and the SD at 50.25° . The trending differences of the two calibration results provide the information that is directly related to on-orbit changes in the RVS. Figure 3 shows the SD and lunar gain trending for MODIS bands 1 and 8. For both Terra and Aqua MODIS, the shortest wavelengths have experienced the most gain and RVS changes. To date, the band 8 (412 nm) gains have changed (decreased) up to 40% for Terra MODIS and more than 45% for Aqua MODIS based on their SD and lunar calibrations. In comparison, the NIR band 1 (646 nm) shows a gain change of less than 20%. The temporal divergence between the SD and lunar gain measurements is a result of the evolution of the on-orbit RVS. Accurate characterization of the on-orbit RVS is extremely important for the MODIS RSB on-orbit calibration, especially for the short wavelength bands.

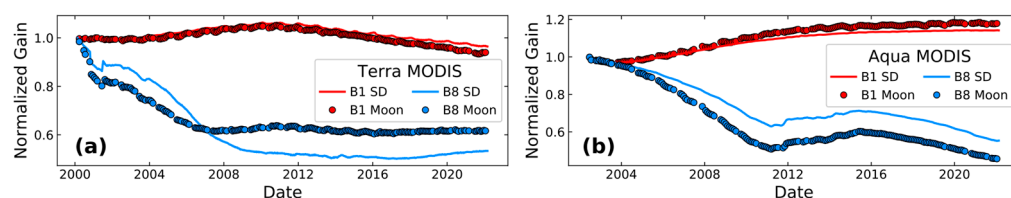


Figure 3. (a) Terra and (b) Aqua MODIS SD and Lunar gain trending for bands 1 and 8.

Initially, the RSB time-dependent RVS was derived by using the lunar and SD calibration differences with an approximation that the RVS on-orbit change for a given RSB is a linear function of the AOI. As each mission continues to operate beyond its designed lifetime, this approximation no longer meets the L1B calibration accuracy requirements, especially at short wavelengths. As a result, the EV response trends at multiple AOIs have been used together with on-orbit SD and lunar measurements to track on-orbit changes in the RVS for a few select bands, starting from L1B Collection 6 (C6) for both Terra and

Aqua MODIS. In C6, we note that the lunar results are not used for bands 1 and 2 EV time-dependent RVS derivation due to the disagreement of lunar measurements with the EV response trending from the desert sites [53].

2.2. VIIRS

Similar to MODIS, a simple smooth function is applied to establish the relationship between the incident radiance and detector digital response for the VIIRS RSB. For all SNPP VIIRS RSB and N20 VIIRS VIS and NIR bands, a quadratic approximation is applied, while for N20 VIIRS SWIR a third order polynomial is used due to a significant nonlinearity effect for these bands [54]. The relationship between the incident radiance and instrument response for the VIIRS RSBs can be written as

$$L = \frac{F \sum_i c_i \cdot dn^i}{RVS} \quad (6)$$

where c_i ($i = 0, 1, 2, 3$), are the prelaunch measured calibration coefficients of the polynomial, F , called F-factor, which is the ratio of the on-orbit coefficients of the polynomial at the time of the measurement to the prelaunch coefficients, assuming that the coefficients of the polynomial change proportionally with each other on-orbit, dn is the background subtracted instrument response, and RVS is the response versus scan angle of the half-angle mirror (HAM). The calibration coefficients, c_0 , c_1 , c_2 , and c_3 , are instrument and electronic temperature-dependent. Both F and the RVS in Equation (6) may, in principle, change temporally on-orbit. However, there is no evidence to suggest that the RVS has a noticeable on-orbit change for either VIIRS instrument. As a result, only the F -factors have been updated regularly on-orbit by using SD and lunar calibrations on an as-needed basis. For the VIIRS EV, the TOA radiance is the primary L1B product, which can be easily converted to its TOA reflectance factor. The VIIRS L1B products are also referred to as the sensor data records (SDR).

VIIRS has the same type of SD as MODIS. The radiance of the sunlight diffusely reflected from the VIIRS SD can also be calculated by Equation (2). The VIIRS SD BRDF, ρ_{SD} , and the SDS transmittance, τ_{SDS} , were measured prelaunch and refined on orbit by measurements made during yaw maneuvers. The VIIRS SD degradation is tracked by the on-board SDSM at eight discrete wavelengths, compared to MODIS at nine different wavelengths of the same spectral range. The VIIRS SD port has a permanently fixed attenuation screen, but it does not have a dedicated door cover as MODIS does. This means that the SD is illuminated by the Sun every orbit. The assumption applied to the MODIS SD calibration that the SD degrades uniformly with respect to incident and outgoing directions is also initially applied to the VIIRS SD calibration. However, there is evidence of non-uniform degradation based on the differences between the lunar and SD trends as will be discussed below.

Comparing the predicted solar radiance (L_{SD}) with that measured using Equation (6) via detector response (dn_{SD}) to the SD, the F-factors for the VIIRS RSB calibration can be calculated by

$$F = \frac{RVS_{SD} \int RSR(\lambda, t) \cdot L_{SD}(\lambda) d\lambda}{[\sum_i c_i dn_{SD}^i] \int RSR(\lambda, t) d\lambda} \quad (7)$$

where RVS_{SD} is the RVS at the AOI of the SD. The VIIRS RSB calibration is performed for each scan using the detector's average response to the SD averaged over the scans in a selected illumination angle range, known as the "sweet spot". The $RSR(\lambda, t)$ in Equation (7) is time-dependent for SNPP VIIRS RSBs as a result of the wavelength-dependent degradation in SNPP rotating telescope assembly (RTA) optics and large OOB RSR contributions [52,55]. The SD calibration is performed for each orbit and the F-factor is derived for each RSB detector, HAM side, and gain stage for the dual gain bands. Compared to Equation (4), designed to derive the MODIS RSB reflectance calibration coefficient, Equation (7) is used to compute the radiance calibration coefficients for the VIIRS RSB. In addition to the SD

bi-directional reflectance function and solar attenuation screen transmission, the sensor's solar spectral irradiance is also needed to determine the predicted radiance reflected off the SD (L_{SD}) used to compute the F in Equation (7). The SNPP uses Kurucz spectra from MODTRAN 4.3 while N20 uses the Thuillier spectra [56].

Applying Equation (6) to the SV lunar observations, the integrated lunar irradiance measured by a VIIRS RSB can be calculated using

$$I = \frac{1}{N} \frac{F \sum_i c_i d n_{Moon}^i \omega}{RVS_{SV}} \quad (8)$$

where $\omega = (S/824)^2$ is the solid angle (steradians) of each pixel of the band. S is 0.375 km for an I-band and 0.75 km for an M-band and 824 km is the nominal orbital altitude. The VIIRS SV has the same AOI as its SD as shown in Figure 1b, at which the RSB RVS is normalized; thus, the RVS_{SV} in Equation (8) is equal to 1. Similar to the lunar calibration for MODIS, the VIIRS lunar calibrations use only the N scans in which the full disk of the Moon can be observed during each scheduled lunar observation. For all regularly scheduled lunar observations of both SNPP and N20 VIIRS, the gain stages of all dual-gain bands are fixed at high gain. Examples of SNPP lunar images for bands I1 and M1 are also shown in Figure 2. For VIIRS lunar observations, only band M7 in N20 has shown any signs of saturation, and even then, for only a few pixels. To correct this, the same approach as used for MODIS bands 13–16 is employed, this time with band M5 as a reference. Similar to the MODIS configuration, a sector rotation is applied to collect lunar data in the EV data sector. However, the VIIRS EV has three different aggregation regions. SNPP and N20 VIIRS lunar data are collected in different aggregation regions and special attention should be paid to the summation over pixels along the scan direction in Equation (8). In this analysis, prelaunch RVS and C2 F -factor LUTs are applied in Equation (8) for SNPP and C2.1 LUTs for N20 VIIRS.

Same as for the MODIS RSBs, the impact of the detector difference on the calibration coefficients derived from a lunar observation for a VIIRS RSB can be assumed to be negligible. Then the detector-averaged relative F factor can be derived from each of the scheduled lunar observations using

$$F^{Moon} = \frac{I N}{\sum_i c_i d n_{Moon}^i}. \quad (9)$$

The predicted lunar irradiance for each lunar observation event, I , is provided by the ROLO model. To distinguish the F -factor derived from the SD/SDSM calibration, a superscript "Moon" is added to the F . Similar to MODIS, the VIIRS lunar calibration is only used to track its RSB on-orbit changes and some of the constant parameters in Equation (8) are dropped in Equation (9). The VIIRS lunar calibration coefficients are scaled by normalizing the lunar F -factors derived from Equation (8) to the corresponding F -factors derived from the SD/SDSM calibration at the time of instrument launch to obtain absolute values of the lunar calibration coefficients.

VIIRS RSBs view the SD and the SV at same AOI of the HAM and thus the SD calibration and lunar calibration should provide identical on-orbit changes for the RSBs if both the SD and lunar calibration results are accurate. It is known that the SD degrades non-uniformly with respect to incident and outgoing direction [45]. Thus, the SD degradation from the SDSM view direction when applied to the RSB view direction may result in long-term biases in the F -factors derived from the SD calibration, especially for short wavelength bands, as also confirmed by EV measurements. A comparison between the two sets of F -factors can identify the long-term biases in the SD F -factors and can be used to obtain the SD degradation differences between the two view directions. Combining the SD and lunar calibration results provides the RSB F -factors with both long-term accuracy and short-term stability.

Similar to the MODIS gains shown in Figure 3, the VIIRS gains are shown in Figure 4 for the VIS band M1 (412 nm) and NIR band I1 (645 nm). Unlike the RVS -caused separation

between the lunar and SD gains in MODIS, the separation between the two sources is a result of the inadequacy in SDSM to accurately characterize the non-uniform degradation in the SD, which manifests as a divergence with the lunar gain. The lunar data can be used as a method for correcting the SD degradation trends so that the SD and lunar trends agree.

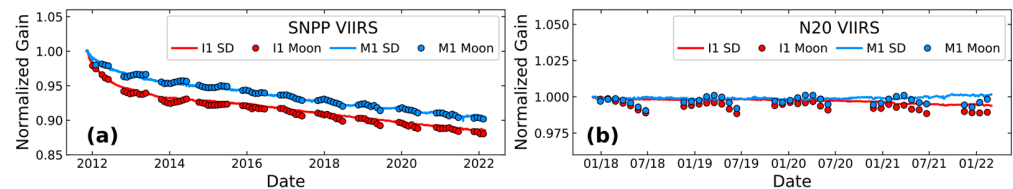


Figure 4. (a) SNPP and (b) N20 VIIRS SD and Lunar gain trending for bands I1 and M1.

3. Calibration Inter-Comparison Using Lunar Observations

Calibration inter-comparisons of two sensors are often made using their near simultaneous nadir observations (SNO) or via measurements over pseudo-invariant EV targets, such as deep convective clouds (DCC) and carefully selected desert sites [57]. In addition to sensor-specific RSR and calibration reference (e.g., the solar spectral irradiance applied for the RSB calibration and retrieval), these approaches often require corrections to reduce the effects due to the variability of atmospheric dynamics and surface reflectance properties involved in the observations. In this study we used lunar observations made by the MODIS and VIIRS instruments to assess their calibration consistency. One of the advantages of using the Moon as a calibration or common reference target for sensor on-orbit calibration is that no atmospheric correction is needed. Plus, the lunar surface reflectance property is extremely stable and depends only on the viewing geometry that can be accurately predicted by a lunar model. This lunar calibration inter-comparison approach was initially developed and applied for assessing the Terra and Aqua MODIS calibration consistency [39]. We extended its application to VIIRS and to a calibration inter-comparison between the MODIS and VIIRS instruments.

In this study, the integrated lunar irradiances, I_{Meas_A} and I_{Meas_B} , measured by sensors A and B were used to perform their calibration inter-comparison via the following ratio ($R_{A/B}$),

$$R_{A/B} = \frac{I_{Meas_A}/I_{Model_A}}{I_{Meas_B}/I_{Model_B}} \quad (10)$$

where I_{Model_A} and I_{Model_B} are the model-predicted lunar irradiances for the corresponding sensor lunar observations. The reference or normalization to the model-predicted lunar irradiances corrects for the effects due to lunar viewing geometry differences between observations and the impact due to sensor-specific RSR as it is part of the input parameters for the lunar model to generate predicted lunar irradiance for a given lunar calibration event. Both MODIS and VIIRS use the same ROLO model for their lunar calibrations. The measured lunar irradiances by MODIS and VIIRS can be computed using Equations (4) and (8), respectively.

Equation (10) can be used for the calibration inter-comparison of two MODIS instruments, which use the same solar spectral irradiance in their RSB calibration. For SNPP and N20 VIIRS, an additional correction is needed to address their solar spectra differences. This correction is also needed for MODIS and VIIRS calibration inter-comparison. Figure 5a illustrates the normalized solar spectrum adopted by MODIS and two VIIRS instruments and their RSB center wavelength locations. We also show data from the TSIS-1 Hybrid Solar Reference Spectrum (HSRS). Figure 5b shows the percent differences between each of the instrument LUTs and the TSIS-1 HSRS. Examples of MODIS (bands 1 and 8) and VIIRS (bands M1 and I1) RSR are shown in Figure 6. In general, Terra and Aqua MODIS RSB RSR are very similar. However, there are small but noticeable differences between SNPP and N20 VIIRS RSB RSR, resulting from sensor build-to-build differences. Both MODIS and VIIRS RSR were well characterized during their pre-launch testing campaign

phases [25,58–60]. For SNPP, an on-orbit modulation is applied to the pre-launch RSR in response to strong wavelength-dependent degradation of its RTA optics [55].

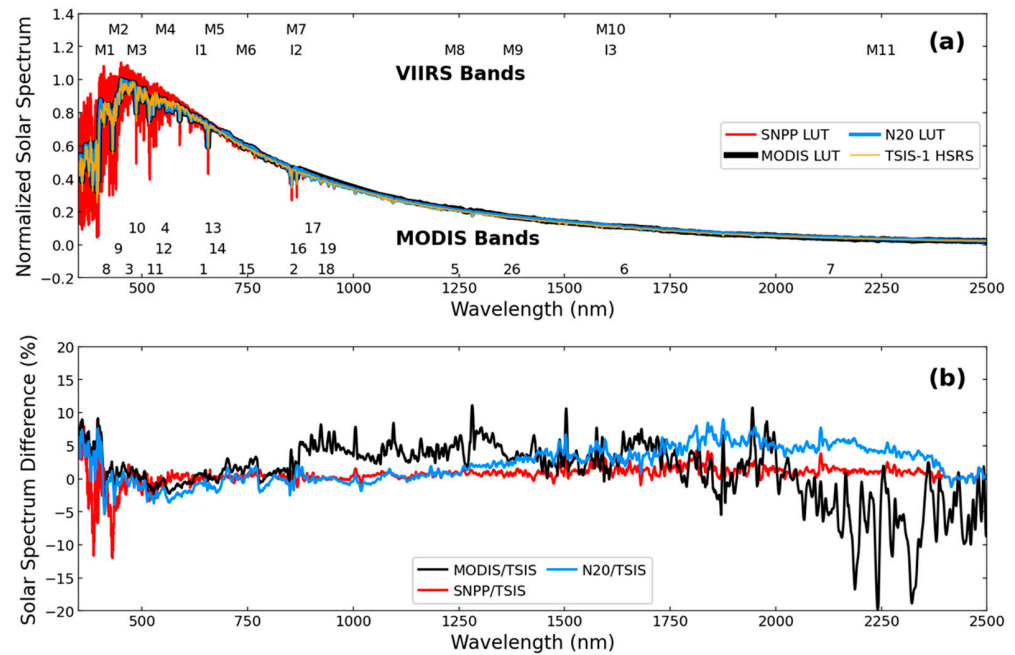


Figure 5. (a) Solar spectrum for MODIS (same for both Terra and Aqua), SNPP VIIRS, N20 VIIRS, and the TSIS-1 HSRS. The data were normalized to the peak value of the MODIS LUT. Band locations are marked according to their wavelengths at the top (VIIRS) or bottom (MODIS) of the figure. (b) Percentage difference of each of the instrument solar spectrum LUTs compared to the TSIS-1 HSRS data. A 10 nm smoothing window was applied to these differences for clarity at the lower wavelengths.

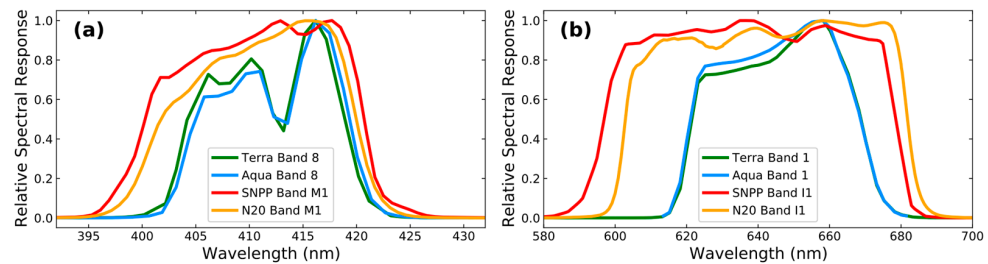


Figure 6. RSR comparison for bands in all four instruments near (a) 410 nm and (b) 640 nm.

By including a correction to remove the calibration difference resulting from the use of different solar spectra by sensors *A* and *B*, the calibration difference between sensors *A* and *B* described by Equation (10) needs to be modified as,

$$R_{A/B}^* = C_{A/B} \cdot R_{A/B} \quad (11)$$

where

$$C_{A/B} = \frac{\int RSR_A(\lambda) E_{SUN_B}(\lambda) d\lambda / \int RSR_A(\lambda) d\lambda}{\int RSR_A(\lambda) E_{SUN_A}(\lambda) d\lambda / \int RSR_A(\lambda) d\lambda} \quad (12)$$

is the correction factor that depends on sensor-specific solar spectra (E_{Sun}) and RSR. The solar spectral reference used in the lunar model has no impact on this inter-comparison approach as long as the same lunar model is used to provide the predicted lunar irradiances for both sensors.

Ideally, if all sensors use the same solar spectra, as recommended by the international Earth-observation calibration and validation communities, such as the Committee on Earth

Observation Satellites (CEOS) Working Group on Calibration and Validation (WGCV) and the Global Space-based Inter-Calibration System (GSICS), the calibration inter-comparisons between two sensors will become more straightforward and accurate and require no additional correction. As an illustration, we also performed a calibration inter-comparison using lunar irradiances generated by using a set of new calibration coefficients and parameters derived by applying the same reference solar spectra for all MODIS and VIIRS instruments. The TSIS-1 HSRS [60], which is a recommended reference spectrum by the CEOS WGCV and GSICS community, will be used in this demonstration. The inter-comparison results from this exercise where all sensor calibrations are referenced to a common solar spectrum will be used to validate the results derived from current calibration approach tied to sensor specific solar spectrum.

4. Results and Discussion

Inter-comparison analyses between the two MODIS and two VIIRS instruments first require a comparison of sensor-measured lunar irradiances with predicted values by the lunar model. This study used the USGS ROLO model to provide the predicted lunar irradiances. While the ROLO model is used to correct for differences in view geometry, particularly the differences in the Earth–Sun and Earth–Moon distances and the lunar phase and libration angles, each mission uses scheduled spacecraft roll maneuvers to constrain the phase angles within a small range. For some bands, this constraint provides a significant improvement in the consistency of the measured and modeled data [61]. Table 2 shows a summary of the number of scheduled lunar events for each instrument along with the roll angle and nominal phase angle ranges in which these rolls are constrained. Over the years, the phase angle criterion is occasionally relaxed when the desired phase angle is outside of the roll angle range. These events are also counted among those reported in Table 2. Typically, both the MODIS and VIIRS instruments acquire 9 to 10 scheduled lunar rolls per year. Only the lunar measurements in the nominal ranges, made by all four instruments between 1 January 2018 and 1 July 2022, were used in this study for the calibration inter-comparison of both MODIS and VIIRS instruments. During this period, Terra, Aqua, SNPP, N20 made 41, 47, 37, and 38 lunar observations, respectively. The difference in their scheduled lunar calibration events is a result of orbit geometry differences, spacecraft operation constraints, and occasionally, other instrument-related activities or events.

Table 2. Summary of scheduled lunar events for MODIS and VIIRS instruments. The number of events listed is from the beginning of each mission through 1 July 2022.

Instrument	Launch Year	Roll Angle Range	Phase Angle Range	Number of Events	Number of Events Outside the Nominal Range
Terra MODIS	1999	−20° to 0°	55° to 56°	216	42
Aqua MODIS	2002	−20° to 0°	−55° to −56°	205	48
SNPP VIIRS	2011	−14° to 0°	−50.5° to −51.5°	90	20
N20 VIIRS	2017	−14° to 0°	−50.5° to −51.5°	39	8

Figure 7 shows the sensor-measured and model-predicted lunar irradiances for Aqua MODIS bands 1 and 8 and for SNPP VIIRS bands I1 and M1 using their regularly scheduled lunar observations over their respective missions. For the measured data, the time-dependent calibration coefficients m_1 and RVS were applied for MODIS and F for VIIRS. Both the measurements and the model predictions show large and similar seasonal oscillations, which are associated with changes in the view geometry, primarily the Earth–Sun and Earth–Moon distances. While the seasonal variation of the measured and modeled data is nearly the same, there is a wavelength-dependent bias between the measurements and the ROLO model, where the MODIS and VIIRS measurements are generally higher than the ROLO predictions. The gaps in the data occur when the geometry of the lunar orbit moves the Moon out of the roll angle range specified in Table 2.

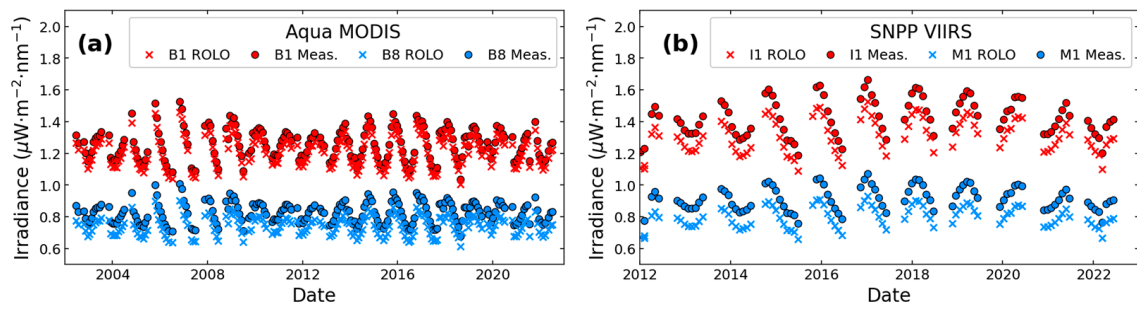


Figure 7. Comparison of the measured lunar irradiance (circles) and ROLO model predicted irradiance (x's) for (a) Aqua MODIS bands 1 and 8 and (b) SNPP VIIRS bands I1 and M1.

We used the time series of ratios of the measured to the predicted lunar irradiances to assess instrument calibration performance. When the pre-launch calibration coefficients were used in the measured data, the ratio was a measure of the trending gain of each band at the AOI of the SV. When the on-orbit coefficients were used, the trending data represent the residual gain change in the instrument, with the expectation that well calibrated data will be flat over long periods. The absolute offset shows the bias between the sensor-measured and the model-predicted data. It depends on the uncertainties in the lunar measurements and the model. As expected, the absolute differences between the model-predicted and sensor-measured irradiance should have little impact on calibration-stability monitoring. Apart from the correction for the view geometry, the use of the ROLO model allowed us to compare bands of different instruments by accounting for the differences in their RSR [62]. In Figure 8, we show the ratio of measured to model trends for bands centered at $0.412\ \mu\text{m}$ (band 8 in MODIS, M1 in VIIRS) and $0.640\ \mu\text{m}$ (band 1 in MODIS, I1 in VIIRS). For each band, the trend of the ratios is stable over the select time series. Each band also shows small seasonal oscillations on the order of 1%, which are associated with residual uncertainties in the ROLO model lunar libration angle correction. For most spectral bands, Terra, Aqua, and N20 are generally in good agreement; however, SNPP shows an offset with the other instruments.

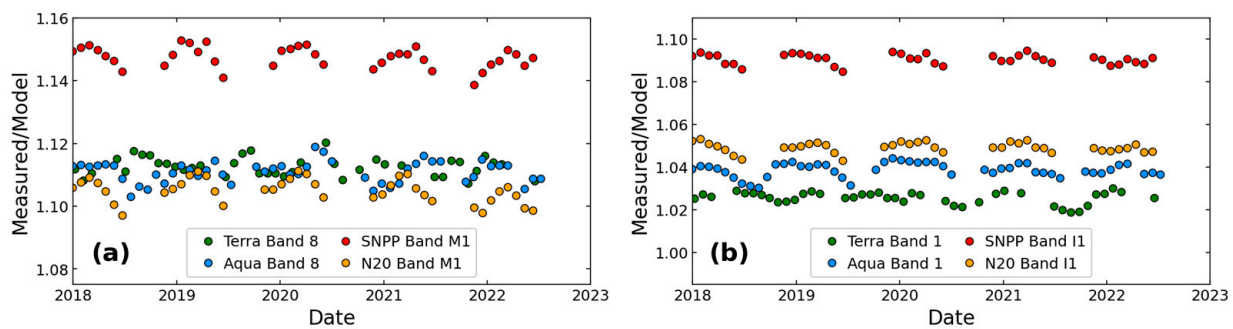


Figure 8. Trending measured/model data for bands in all four instruments near (a) $0.412\ \mu\text{m}$ (MODIS band 8, VIIRS Band M1) and (b) $0.640\ \mu\text{m}$ (MODIS Band 1, VIIRS Band I1).

In Figure 9, we show the mean values of the measured/model data of MODIS and VIIRS VIS/NIR bands from 1 January 2018 to 1 July 2022. For each instrument, the ratios are lower in the middle wavelength range compared to the data at other wavelengths. At shorter wavelengths, Terra, Aqua, and N20 are in better agreement compared to SNPP except for band M2, which has a similar ratio to MODIS band 9. MODIS band 12 also shows a higher ratio than MODIS band 4 and N20 band M4 at a similar wavelength. For the high gain ocean bands of MODIS (13–16), the impact of saturation could lead to more disagreement over that wavelength range, particularly for Aqua MODIS with more saturated lunar pixels that require a correction [51].

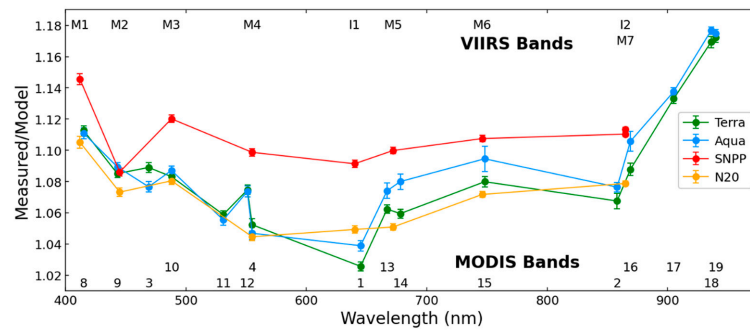


Figure 9. Ratio of the measured data and the ROLO model data as a function of wavelength for the VIS/NIR bands in both MODIS and VIIRS. The ratios are taken from data between 1 January 2018 and 1 July 2022 as shown in Figure 8. The error bars show the standard deviation.

With the exception of small residual uncertainties among different lunar phases and libration angles, the absolute uncertainty of the lunar model is cancelled in this lunar calibration inter-comparison. In this study, we have used a large number of lunar observations made at nearly the same phase angles and the impact due to small residual uncertainties in the lunar model is therefore minimized. Presented in Tables 3–5 are the lunar calibration inter-comparison results for Terra and Aqua MODIS, SNPP and N20 VIIRS, and Aqua MODIS and N20 VIIRS, respectively, using their regularly scheduled lunar observations made between 1 January 2018 and 1 July 2022. The results for SNPP and N20 VIIRS and for Aqua MODIS and N20 VIIRS include a correction (Equation (11)) to remove the impact due to different solar spectra used in their on-orbit calibration. It requires no additional correction for Terra and Aqua MODIS lunar calibration inter-comparison as both use the same solar spectra. The calibration differences (DIF) in these tables, expressed in percentage (%), were computed using the averages of measured/predicted ratios of the same (or matching) spectral bands from the two instruments (i.e., $DIF = (R_{A/B}^* - 1) \times 100$). The standard deviations reported in the tables are the combined values based on their time-series.

Table 3. Lunar calibration inter-comparison results for Terra and Aqua MODIS (WL: wavelength; DIF: difference (Terra—Aqua); STD: standard deviation; UC: uncertainty). The values are listed as a percentage and the uncertainties were propagated from the values for each instrument/band listed in Table 6.

Band	01	02	03	04	08	09	10	11
WL (μ)	0.65	0.86	0.47	0.56	0.41	0.44	0.49	0.53
DIF	−1.27	−0.82	1.15	0.52	0.15	−0.40	−0.37	0.33
STD	0.43	0.56	0.45	0.56	0.45	0.37	0.40	0.42
UC	2.92	3.01	2.48	2.32	2.43	2.31	2.26	2.26
Band	12	13	14	15	16	17	18	19
WL (μ)	0.57	0.65	0.68	0.75	0.87	0.91	0.94	0.94
DIF	0.09	−1.09	−1.90	−1.34	−1.63	−0.40	−0.62	−0.21
STD	0.46	0.55	0.56	0.86	0.74	0.41	0.44	0.41
UC	2.25	2.40	2.41	2.44	2.56	2.32	2.38	2.33

Table 4. Lunar calibration inter-comparison results for SNPP and N20 VIIRS (WL: wavelength; DIF: difference (SNPP—N20); STD: standard deviation; UC: uncertainty). The values are listed as a percentage and the uncertainties were propagated from the values for each instrument/band listed in Table 7.

Band	M1	M2	M3	M4	I1	M5	M6
WL (μ)	0.41	0.45	0.49	0.56	0.64	0.67	0.75
DIF	3.78	3.41	3.09	3.14	2.41	2.64	2.89
STD	0.50	0.37	0.34	0.33	0.33	0.29	0.28
UC	2.04	2.02	1.95	1.94	1.91	1.95	2.05

Table 4. *Cont.*

Band	M1	M2	M3	M4	I1	M5	M6
Band	I2	M7	M8	M9	I3	M10	M11
WL (μ)	0.87	0.87	1.24	1.38	1.61	1.61	2.25
DIF	2.93	2.95	3.70	2.98	3.30	2.56	2.56
STD	0.17	0.20	0.29	0.33	0.31	0.32	0.45
UC	1.95	1.92	2.02	2.07	2.68	2.01	2.70

Table 5. Lunar calibration inter-comparison results for Aqua MODIS and N20 VIIRS (WL: wavelength; DIF: difference (Aqua—N20); STD: standard deviation; UC: uncertainty). The values are listed as a percentage and the uncertainties were propagated from the values for each instrument/band listed in Tables 6 and 7.

Bands	8/M1	9/M2	3/M3	4/M4	1/I1	13/M5	15/M6	2/I2	16/M7
DIF	−0.86	0.11	−1.73	−1.17	−2.37	0.77	0.72	−2.63	0.24
STD	0.51	0.39	0.40	0.46	0.40	0.52	0.81	0.31	0.65
UC	2.14	2.07	2.14	2.08	2.41	2.12	2.17	2.49	2.21

Table 6. Terra and Aqua MODIS lunar calibration uncertainty. The uncertainties are listed as a percentage.

Band	Terra MODIS				Aqua MODIS			
	U ₁	U ₂	U ₃	Total	U ₁	U ₂	U ₃	Total
1	1.60	1.20	0.53	2.07	1.6	1.23	0.43	2.06
2	1.66	1.27	0.31	2.11	1.63	1.38	0.25	2.15
3	1.55	0.30	0.82	1.78	1.53	0.5	0.63	1.73
4	1.51	0.23	0.57	1.63	1.52	0.51	0.42	1.66
8	1.62	0.37	0.53	1.74	1.58	0.35	0.51	1.70
9	1.60	0.30	0.30	1.66	1.57	0.24	0.24	1.61
10	1.59	0.21	0.21	1.62	1.56	0.22	0.14	1.58
11	1.58	0.26	0.16	1.61	1.56	0.24	0.1	1.58
12	1.57	0.26	0.16	1.60	1.56	0.24	0.09	1.58
13	1.59	0.26	0.09	1.69	1.59	0.36	0.05	1.71
14	1.59	0.27	0.09	1.69	1.59	0.39	0.05	1.71
15	1.59	0.31	0.10	1.70	1.59	0.52	0.06	1.75
16	1.69	0.32	0.08	1.79	1.67	0.54	0.05	1.83
17	1.62	0.14	0.26	1.65	1.6	0.24	0.21	1.63
18	1.64	0.23	0.34	1.69	1.63	0.27	0.31	1.68
19	1.62	0.18	0.27	1.65	1.61	0.25	0.23	1.65

Table 7. SNPP and N20 VIIRS lunar calibration uncertainty. The uncertainties are listed as a percentage.

Band	SNPP VIIRS				N20 VIIRS			
	U ₁	U ₂	U ₃	Total	U ₁	U ₂	U ₃	Total
I1	1.44	0.01	0.21	1.46	1.22	0.01	0.21	1.24
I2	1.43	0.02	0.40	1.49	1.21	0.02	0.32	1.25
I3	1.60	0.10	1.31	2.07	1.22	0.10	1.19	1.71
M1	1.50	0.00	0.45	1.57	1.26	0.02	0.34	1.30
M2	1.49	0.00	0.42	1.54	1.25	0.01	0.39	1.31
M3	1.46	0.00	0.27	1.49	1.24	0.01	0.22	1.26
M4	1.45	0.02	0.30	1.48	1.23	0.02	0.26	1.26

Table 7. Cont.

Band	SNPP VIIRS				N20 VIIRS			
	U ₁	U ₂	U ₃	Total	U ₁	U ₂	U ₃	Total
M5	1.44	0.11	0.38	1.50	1.22	0.09	0.27	1.26
M6	1.44	0.49	0.50	1.60	1.22	0.10	0.40	1.29
M7	1.44	0.22	0.22	1.47	1.22	0.11	0.19	1.24
M8	1.60	0.03	0.19	1.61	1.22	0.03	0.12	1.22
M9	1.60	0.08	0.40	1.65	1.22	0.05	0.26	1.25
M10	1.60	0.04	0.11	1.60	1.22	0.02	0.08	1.22
M11	1.60	0.57	0.16	1.70	2.09	0.03	0.15	2.10

For Terra and Aqua MODIS, their lunar calibration inter-comparison results (Table 3) indicate that their on-orbit calibration consistency is generally within 1%, with exceptions for a few bands (1, 3, 13–16) that are within 2%. As discussed earlier, the high-gain ocean bands (13–16) have utilized a correction to mitigate the impact due to some saturated pixels in their lunar images. Unlike MODIS, the two VIIRS instruments (Table 4) show noticeably large calibration differences, ranging from 2.4% (I1) to 3.8% (M1), with SNPP reporting higher radiances than N20. In nearly all cases, the standard deviations in the VIIRS lunar measurement time series are smaller than MODIS, indicating a better calibration stability. Large calibration differences between the two VIIRS instruments are a known issue found shortly after the N20 VIIRS began its nominal operation. One of the likely causes is due to errors not identified and accounted for in pre-launch SD BRF and/or screen transmission measurements [63]. Table 5 is a summary of calibration inter-comparison results for several matching VIS/NIR spectral bands of Aqua MODIS and N20 VIIRS. The calibration differences are within 2%, with the exception of band pairs of 1/I1 and 2/I2 being slightly above 2%. Combining results presented in Tables 3–5, one can also derive the calibration differences between Terra MODIS and N20 VIIRS and that between Terra (and Aqua) MODIS and SNPP VIIRS.

The lunar calibration inter-comparison uncertainties are also reported in Tables 3–5. They were derived based on the uncertainties involved in both MODIS and VIIRS lunar irradiance measurements (Equations (4) and (8)), including the uncertainties of their calibration coefficients (m_1 for MODIS and F for VIIRS), the measurement errors of detectors' lunar responses due to detector SNRs, and the RVS uncertainties (for MODIS). Details of MODIS and VIIRS on-orbit calibration uncertainty assessments can be found in the following references [64,65]. In general, the uncertainty was computed as the root mean square (RMS) of the individual uncertainties associated with each term in computing the radiance (Equations (1) and (6)), with the covariance terms between different parameters considered to be negligible. Table 6 provides the uncertainties involved in the MODIS lunar irradiance measurements. The U1 term is the uncertainty in the on-orbit calibration coefficients and includes the uncertainties in the SD BRF characterization, its on-orbit degradation, and SD screen transmission. These terms use constant values and do not change on-orbit. The U2 term is the RVS uncertainty and is both time- and AOI-dependent. The uncertainty for terms derived from time-series data use the standard deviation of the residuals after a piece-wise fit to the data. The U3 term represents the uncertainty related to detector lunar responses, which accounts for the uncertainty in the instrument temperature correction as well as the signal to noise of each lunar event. For this work, average dn was calculated for each lunar event to compute the signal-to-noise uncertainty. Due to the special effort made to correct saturated pixels in bands 13–16 by referencing a non-saturated band, an extra 0.5% uncertainty is included to their total lunar calibration uncertainties. For VIIRS, the lunar calibration uncertainties shown in Table 7 are generally smaller than MODIS, mainly due to smaller uncertainties reported pre-launch SD BRF characterization. The U2 term in VIIRS is the uncertainty associated with the pre-launch calibration coefficients (c_i) as the on-orbit F-factor (F) is derived by comparing the predicted radiance from the SD with that measured based on pre-launch calibration coefficients (c_i).

The uncertainties shown in Tables 3–5 are the combined lunar measurement uncertainties of the same of matching band pairs. Considering both MODIS and VIIRS have a calibration requirement of 2%, the lunar calibration inter-comparison results for two MODIS instruments and for Aqua MODIS and N20 VIIRS clearly meet their combined calibration requirement of 2.8%. On the other hand, the SNPP and N20 VIIRS calibration is not consistent to within their combined calibration requirement for several VIS/NIR bands. This indicates that the U1 term in Table 7 is probably underestimated for SNPP. As a result, special efforts must be made in order to generate high quality science products using measurements from both VIIRS instruments.

MODIS and VIIRS calibration inter-comparison results can be found in a number of references with most approaches based on the use of simultaneous nadir observations (SNO) and pseudo-invariant targets, such as Libya-4 desert, Dome C, and DCCs, and major efforts made by the NASA and NOAA calibration teams and different science groups [19,26,56,66–68]. As expected, the ground-based approaches can only perform calibration inter-comparison for some of the spectral bands. For Terra and Aqua MODIS, ground-based calibration inter-comparison results are wavelength- and the EV surface property-dependent and, on average, are less than $\pm 1\%$ for most spectral bands, except for band 3 (1.3–2.3%), band 8 (0.5–1.9%), and band 11 (–1.7%). No ground-based inter-comparison results are available for band 13–16 as many pixels over the select EV targets saturate. For SNPP and N20 VIIRS, results from ground-based approaches applied by different groups all indicate large calibration differences for several VIS/NIR bands, which is consistent with the conclusion from lunar calibration inter-comparisons. Vicarious calibration results show that N20 VIIRS reflectances are systematically lower than SNPP by 2 to 4% for most bands, but a larger disagreement (6–7%) is observed for the shortest wavelength bands (M1–M3). For Aqua MODIS and N20 VIIRS, the ground-based calibration inter-comparisons also show larger calibration differences, but smaller than the differences between the two VIIRS instruments. Apart from large standard deviations involved in the EV observations, the results from different vicarious approaches or derived by different groups could vary (up to 1–3%) as it is extremely difficult to make accurate corrections for the surface reflectance profile and atmospheric effect for observations made at different times. The calibration differences could also depend on the L1B data used in the performance assessments, such as the data source and collection.

Finally, we also compared the lunar calibration inter-comparison results derived with all sensors' calibration tied to the same TSIS-1 HSRS, including reprocessing their calibration coefficients and parameters involved in computing the measured lunar irradiances. In this case, Equation (10) can be used directly for lunar calibration inter-comparisons of all instruments. As expected, the results from using the same solar spectrum (i.e., no additional correction needed) for sensor on-orbit calibration are very consistent with those derived using Equation (11), which includes a correction for Equation (10) to remove the calibration impact due to different solar spectra used by individual sensors. For SNPP and N20 VIIRS, the differences between the two approaches are less than 0.2%. For Aqua MODIS and N20 VIIRS, the differences are also very small, except for band pairs of 1/I1 (0.3%), 2/I2 (0.7%), and 8/M1 (0.6%). Both MODIS use the same solar spectrum for their on-orbit calibration and do not require additional correction for their lunar calibration inter-comparison. If all sensors use the same solar spectrum, their on-orbit calibration consistency assessments via vicarious approaches could become much simpler. This could also help improve the quality of the science products generated from different instruments, especially when their measured radiances are involved.

Apart from tying the sensor reflective solar calibration to the same solar spectrum, the absolute accuracy of the reference spectrum is also important as it has direct impact on lunar calibration. This is demonstrated by the reduced differences between the measured and ROLO model predicted lunar irradiances for MODIS bands 17–19. As expected, the TSIS-1 hybrid spectrum is more accurate than the one adopted for MODIS more than 20 years ago, going from the high of around 18% different (shown in Figure 9) down to approximately

12%. The use of the TSIS-1 spectrum has led to a more consistent lunar calibration result among all RSB. Another parameter that could potentially impact the accuracy of lunar calibration inter-comparison is detector's instantaneous field of view (IFOV), which is tied to the solid angle (ω) included in Equations (4) and (8). The IFOV is an important sensor design parameter that is typically characterized during pre-launch measurements. The error in the IFOV characterization could have a few implications for lunar observations in whiskbroom sensors such as MODIS and VIIRS. As an effort to improve our lunar calibration and calibration inter-comparison quality and uncertainty, and to support the development of a lunar model that is not only stable but also more accurate, we have planned for an in-depth investigation of the residual impact due to sensor IFOV on the measured lunar irradiances. This will include the effects of lunar motion during the time of image acquisition, which are expected to be small. We will report our findings once this investigation is complete. We also plan to perform similar lunar calibration and lunar calibration inter-comparisons with JPSS-2 VIIRS scheduled to launch late 2022 to gain a better understanding of the VIIRS calibration differences and to help develop a viable strategy for generating consistent long-term L1B data products from all VIIRS instruments.

5. Conclusions

The high-quality measurements from the two MODIS and two VIIRS instruments, coupled with the extensive and dedicated pre- and post-launch calibration and characterization efforts made by the vendor and government-led calibration teams, have facilitated the production of numerous data products that have advanced the studies of the Earth's system and its environmental parameters. In addition to on-board calibrators, lunar observations have been regularly scheduled and applied to monitor the RSB on-orbit calibration stability. In this paper, an inter-comparison technique of using on-orbit lunar observations was formulated and applied to evaluate the calibration differences between the MODIS and VIIRS instruments. This approach normalizes the measured lunar irradiances from each spectral band with the lunar irradiances obtained from the ROLO model and therefore can correct for the differences caused by the view geometry-specific parameters. An additional correction factor is also included in this approach for lunar calibration inter-comparison of sensors that use different solar irradiance spectra in their on-orbit calibration. The results showed that the Terra and Aqua MODIS RSB on-orbit calibrations agree well to within $\pm 1\%$, except for the NIR high-gain ocean bands (13–16) that are impacted by saturation. Conversely, the two VIIRS instruments showed a noticeable disagreement of 2–4% in the VIS bands, 1–3% in the NIR bands, and 2–3% in the SWIR bands. Aqua MODIS and N20 VIIRS calibrations generally agree to within 2%, except for bands 1/I1 and 2/I2 (~2.5%). SWIR band results were not presented due to electronic crosstalk issues in the MODIS bands. Compared to vicarious approaches, the lunar calibration inter-comparison approach, relying on the superb stability of the lunar surface property, can be easily extended to the calibration stability monitoring and calibration inter-comparisons of future satellite instruments as well, such as the VIIRS on JPSS-2, 3, and 4 and OCI on PACE. As an exercise, this paper has also demonstrated the advantages of using a common and accurate solar irradiance spectrum for all sensors' on-orbit calibrations.

Author Contributions: Conceptualization, X.X.; Data curation, J.S., A.A. and T.W.; Formal analysis, A.A. and T.W.; Methodology, X.X., J.S., A.A. and T.W.; Writing—original draft, X.X.; Writing—review & editing, J.S., A.A. and T.W. All authors have read and agreed to the published version of the manuscript.

Funding: This research received no external funding.

Data Availability Statement: Not applicable.

Acknowledgments: Authors of this paper would like to thank Tom Stone of USGC for regularly providing model lunar irradiances and to acknowledge the current and former members of MODIS and VIIRS Characterization Support Team (MCST/VCST), especially, Jon Fulbright, Zhipeng Wang, and Ning Lei, for their technical assistance and contributions for our lunar calibration tasks. We also greatly appreciate the support from NASA and NOAA Mission Operation Teams for Terra, Aqua, SNPP, and N20 and NOAA SDR calibration team.

Conflicts of Interest: The authors declare no conflict of interest.

References

1. Salomonson, V.; Barnes, W.L.; Maymon, P.W.; Montgomery, H.E.; Ostrow, H. MODIS: Advanced facility instrument for studies of the Earth as a system. *IEEE Trans. Geosci. Rem. Sens.* **1989**, *27*, 145–153. [[CrossRef](#)]
2. Justice, C.; Vermote, E.; Townshend, J.; Defries, R.; Roy, D.; Hall, D.; Salomonson, V.; Privette, J.; Riggs, G.; Strahler, A.; et al. The Moderate Resolution Imaging Spectroradiometer (MODIS): Land Remote Sensing for Global Change Research. *IEEE Trans. Geosci. Remote Sens.* **1998**, *36*, 1228–1249. [[CrossRef](#)]
3. Esaias, E.; Abbott, M.; Barton, I.; Brown, O.; Campbell, J.; Carder, K.; Clark, D.; Evans, R.; Hoge, F.; Gordon, H.; et al. An Overview of MODIS Capabilities for Ocean Science Observations. *IEEE Trans. Geosci. Remote Sens.* **1998**, *36*, 1250–1265. [[CrossRef](#)]
4. King, M.; Menzel, P.; Kaufman, Y.; Tanre, D.; Gao, B.; Platnick, S.; Ackerman, S.; Remer, L.; Pincus, R.; Hubanks, P. Cloud and Aerosol Properties, Precipitable Water, and Profiles of Temperature and Water Vapor from MODIS. *IEEE Trans. Geosci. Remote Sens.* **2003**, *41*, 442–458. [[CrossRef](#)]
5. Remer, L.A.; Kaufman, Y.; Tanré, D.; Mattoo, S.; Chu, D.A.; Martins, J.V.; Li, R.; Ichoku, C.; Levy, R.C.; Kleidman, R.; et al. The MODIS aerosol algorithm, products, and validation. *J. Atmos. Sci.* **2005**, *62*, 947–973. [[CrossRef](#)]
6. Kilpatrick, K.A.; Podestá, G.; Walsh, S.; Williams, E.; Halliwell, V.; Szczodrak, M.; Brown, O.B.; Minnett, P.J.; Evans, R. A decade of sea surface temperature from MODIS. *Remote Sens. Environ.* **2015**, *165*, 27–41. [[CrossRef](#)]
7. Masuoka, E.J.; Roy, D.; Wolfe, R.E.; Morisette, J.; Sinno, S.; Teague, M.; Saleous, N.Z.; Devadiga, S.; Justice, C.O.; Nickeson, J. MODIS Land Data Products: Generation, Quality Assurance and Validation. *Land Remote Sens. Glob. Environ. Chang.* **2010**, *11*, 509–532.
8. Parkinson, C. Aqua: An Earth-Observing Satellite Mission to Examine Water and Other Climate Variables. *IEEE Trans. Geosci. Remote Sens.* **2003**, *41*, 173–183. [[CrossRef](#)]
9. Xiong, X.; King, M.; Salomonson, V.; Barnes, W.; Wenny, B.; Angal, A.; Wu, A.; Madhavan, S.; Link, D. Moderate Resolution Imaging Spectroradiometer on Terra and Aqua Missions. In *Optical Payloads for Space Missions*; Qian, S., Ed.; John Wiley Sons Ltd.: Hoboken, NJ, USA, 2015.
10. Schueler, C.F.; Clement, E.; Ardanuy, P.; Welsh, C.; DeLuccia, F.; Swenson, H. NPOESS VIIRS sensor design overview. In Proceedings of the International Symposium on Optical Science and Technology, San Diego, CA, USA, 18 January 2002; Volume 4483, pp. 11–23.
11. Lee, T.; Miller, S.; Schueler, C.; Miller, S. NASA MODIS previews NPOESS VIIRS capabilities. *Weather Forecast.* **2006**, *21*, 649–655. [[CrossRef](#)]
12. Goldberg, M.D.; Kilcoyne, H.; Cikanek, H.; Mehta, A. Joint Polar Satellite System: The United States next generation civilian polar-orbiting environmental satellite system. *J. Geophys. Res. Atmos.* **2013**, *118*, 13463–13475. [[CrossRef](#)]
13. Justice, C.O.; Román, M.O.; Csiszar, I.; Vermote, E.F.; Wolfe, R.E.; Hook, S.J.; Friedl, M.; Wang, Z.; Schaaf, C.B.; Miura, T.; et al. Land and cryosphere products from Suomi NPP VIIRS: Overview and status. *J. Geophys. Res. Atmos.* **2013**, *118*, 9753–9765. [[CrossRef](#)]
14. Gladkova, I.; Ignatov, A.; Shahriar, F.; Kihai, Y.; Hillger, D.; Petrenko, B. Improved VIIRS and MODIS SST imagery. *Remote Sens.* **2016**, *8*, 79. [[CrossRef](#)]
15. Wang, M.; Jiang, L.; Son, S.; Liu, X.; Voss, K. Deriving consistent ocean biological and biogeochemical products from multiple satellite ocean color sensors. *Opt. Express* **2020**, *28*, 2661–2682. [[CrossRef](#)]
16. Platnick, S.; Meyer, K.; Wind, G.; Holz, R.E.; Amarasinghe, N.; Hubanks, P.A.; Marchant, B.; Dutcher, S.; Veglio, P. The NASA MODIS-VIIRS Continuity Cloud Optical Properties Products. *Remote Sens.* **2020**, *13*, 2. [[CrossRef](#)]
17. Zhou, L.; Divakarla, M.; Liu, X.; Layns, A.; Goldberg, M. An Overview of the Science Performances and Calibration/Validation of Joint Polar Satellite System Operational Products. *Remote Sens.* **2019**, *11*, 698. [[CrossRef](#)]
18. Goldberg, M.D.; Cikanek, H.; Zhou, L.; Price, J. *Comprehensive Remote Sensing Optical Sensors-VIS/NIR/SWIR*; Liang, S., Ed.; Elsevier: Oxford, UK, 2018; Volume 1, pp. 91–118.
19. Meyer, K.; Platnick, S.; Holz, R.; Dutcher, S.; Quinn, G.; Nagle, F. Derivation of Shortwave Radiometric Adjustments for SNPP and NOAA-20 VIIRS for the NASA MODIS-VIIRS Continuity Cloud Products. *Remote Sens.* **2020**, *12*, 4096. [[CrossRef](#)]
20. Turpie, K.R.; Eplee, R.E.; Franz, B.A.; Del Castillo, C. Calibration uncertainty in ocean color satellite sensors and trends in long-term environmental records. *Ocean. Sens. Monit. VI* **2014**, *9111*, 911103.
21. Franz, B.A.; Bailey, S.W.; Werdell, P.J.; McClain, C.R. Sensor-independent approach to the vicarious calibration of satellite ocean color radiometry. *Appl. Opt.* **2007**, *46*, 5068–5082. [[CrossRef](#)]

22. Barnes, B.B.; Hu, C.; Bailey, S.W.; Pahlevan, N.; Franz, B.A. Cross-calibration of MODIS and VIIRS long near infrared bands for ocean color science and applications. *Remote Sens. Environ.* **2021**, *260*, 112439. [[CrossRef](#)]
23. Moon, M.; Zhang, X.; Henebry, G.M.; Liu, L.; Gray, J.M.; Melaas, E.K.; Friedl, M.A. Long-term continuity in land surface phenology measurements: A comparative assessment of the MODIS land cover dynamics and VIIRS land surface phenology products. *Remote Sens. Environ.* **2019**, *226*, 74–92. [[CrossRef](#)]
24. Barnes, W.L.; Salomonson, V.V. MODIS: A global image spectroradiometer for the Earth Observing System. *Crit. Rev. Opt. Sci. Technol.* **1993**, *CR47*, 285–307.
25. Xiong, X.; Chiang, K.; Esposito, J.; Guenther, B.; Barnes, W.L. MODIS On-orbit Calibration and Characterization. *Metrologia* **2003**, *40*, 89–92. [[CrossRef](#)]
26. Xiong, X.; Angal, A.; Chang, T.; Chiang, K.; Lei, N.; Li, Y.; Sun, J.; Twedt, K.; Wu, A. MODIS and VIIRS calibration and characterization in support of producing long-term high-quality data products. *Remote Sens.* **2020**, *12*, 3167. [[CrossRef](#)]
27. Xiong, X.; Wilson, T.; Angal, A.; Sun, J. Using the moon and stars for VIIRS day/night band on-orbit calibration. In Proceedings of the SPIE 11151, Sensors, Systems, and Next-Generation Satellites XXIII, Strasbourg, France, 10 October 2019; p. 111511Q.
28. Sun, J.; Xiong, X.; Barnes, W.; Guenther, B. MODIS Reflective Solar Bands On-orbit Lunar Calibration. *IEEE Trans. Geosci. Remote Sens.* **2007**, *45*, 2383–2393. [[CrossRef](#)]
29. Xiong, X.; Sun, J.; Fulbright, J.; Wang, Z.; Butler, J. Lunar Calibration and Performance for S-NPP VIIRS Reflective Solar Bands. *IEEE Trans. Geosci. Remote Sens.* **2016**, *54*, 1052–1061. [[CrossRef](#)]
30. Eplee, R.E.; Turpie, K.R.; Meister, G.; Patt, F.S.; Franz, B.A.; Bailey, S.W. On-orbit calibration of the Suomi national polar-orbiting partnership visible infrared imaging radiometer suite for ocean color applications. *Appl. Opt.* **2015**, *54*, 1984–2006. [[CrossRef](#)]
31. Kieffer, H.; Stone, T.C. The Spectral Irradiance of the Moon. *Astron. J.* **2005**, *129*, 2887. [[CrossRef](#)]
32. Stone, T.C.; Kieffer, H.H. Use of the Moon to support on-orbit sensor calibration for climate change measurements. In Proceedings of the SPIE—Earth Observing Systems XI, San Diego, CA, USA, 14–16 August 2006; Volume 6296.
33. Stone, T.C.; Kieffer, H.; Lukashin, C.; Turpie, K. The Moon as a climate-quality radiometric calibration reference. *Remote Sens.* **2020**, *12*, 1837. [[CrossRef](#)]
34. Barnes, R.A.; Eplee, R.E.; Patt, F.S.; McClain, C.R. Changes in the radiometric sensitivity of SeaWiFS determined from lunar and solar-based measurements. *Appl. Opt.* **1999**, *38*, 4649–4664. [[CrossRef](#)]
35. Markham, B.; Barsi, J.; Kvaran, G.; Ong, L.; Kaita, E.; Biggar, S.; Myers, J.C.; Mishra, N.; Helder, D. Landsat-8 operational land imager radiometric calibration and stability. *Remote Sens.* **2014**, *6*, 12275–12308. [[CrossRef](#)]
36. Shao, X.; Cao, C.; Upreti, S.; Padula, F.; Choi, T. Comparing Hyperion Lunar Observation with model calculations in support of GOES-R Advanced Baseline Imager (ABI) calibration. *Earth Obs. Syst.* **2014**, *XIX*, 9218, 92181X.
37. Lachérade, S.; Fourest, S.; Gamet, P.; Lebègue, L. PLEIADES absolute calibration: Inflight calibration sites and methodology. *PAN* **2012**, *1* (B2), B3. [[CrossRef](#)]
38. Xiong, X.; Wang, Z.; Sun, J.; Angal, A.; Fulbright, J.; Butler, J. MODIS and VIIRS lunar observations and applications. *Sens. Syst. Next-Gener. Satell.* **2013**, *XVII*, 8889, 175–185.
39. Xiong, X.; Sun, J.; Barnes, W. Intercomparison of on-orbit calibration consistency between Terra and Aqua MODIS reflective solar bands using the moon. *IEEE Geosci. Remote Sens. Lett.* **2008**, *5*, 778–782. [[CrossRef](#)]
40. Wang, Z.; Xiong, X.; Li, Y. Improved band-to-band registration characterization for VIIRS reflective solar bands based on lunar observations. *Remote Sens.* **2015**, *8*, 27. [[CrossRef](#)]
41. Wilson, T.; Xiong, X. Modulation transfer function characterization for GOES-16 Advanced Baseline Imager using lunar observations. *Earth Obs. Syst.* **2019**, *XXIV*, 11127, 460–467.
42. Li, Y.; Xiong, X. Monitoring VIIRS thermal emissive bands long-term performance using lunar observations. *Sens. Syst. Next-Gener. Satell.* **2020**, *XXIV*, 11530, 286–294.
43. Wilson, T.; Wu, A.; Shrestha, A.; Geng, X.; Wang, Z.; Moeller, C.; Frey, R.; Xiong, X. Development and implementation of an electronic crosstalk correction for bands 27–30 in Terra MODIS collection 6. *Remote Sens.* **2017**, *9*, 569. [[CrossRef](#)]
44. Xiong, X.; Chiang, K.; Adimi, F.; Li, W.; Yatagi, H.; Barnes, W. MODIS correction algorithm for out-of-band response in the short-wave IR bands. *Sens. Syst. Next-Gener. Satell.* **2004**, *VII*, 5234, 605–614.
45. Lei, N.; Xiong, X.; Wang, Z.; Li, S.; Twedt, K. SNPP VIIRS RSB on-orbit radiometric calibration algorithms Version 2.0 and the performances, part 1: The algorithms. *J. Appl. Remote Sens.* **2020**, *14*, 047501. [[CrossRef](#)]
46. Twedt, K.; Lei, N.; Xiong, X.; Angal, A.; Li, S.; Chang, T.; Sun, J. On-orbit Calibration and Performance of NOAA-20 VIIRS Reflective Solar Bands. *IEEE Trans. Geosci. Remote Sens.* **2022**, *60*, 1001413. [[CrossRef](#)]
47. Xiong, X.; Sun, J.; Esposito, J.; Liu, X.; Barnes, W.L.; Guenther, B. On-orbit Characterization of a Solar Diffuser’s Bi-directional Reflectance Factor Using Spacecraft Maneuvers. In *Proceedings of SPIE—Earth Observing Systems VIII*; SPIE Press: Bellingham, DC, USA, 2003; Volume 5151, pp. 375–383.
48. Twedt, K.; Aldoretta, E.; Angal, A.; Chen, H.; Geng, X.; Li, Y.; Mu, Q.; Vermeesch, K.; Xiong, X. MODIS reflective solar bands calibration improvements for Collection 7. *Sens. Syst. Next-Gener. Satell.* **2021**, *XXV*, 11858, 118580S.
49. Xiong, X.; Angal, A.; Twedt, K.A.; Chen, H.; Link, D.; Geng, X.; Aldoretta, E.; Mu, Q. MODIS Reflective Solar Bands On-orbit Calibration and Performance. *IEEE Trans. GeoScience Remote Sens.* **2019**, *57*, 6355–6371. [[CrossRef](#)]
50. Kieffer, H. Photometric Stability of the Lunar Surface. *Iracus* **1997**, *130*, 323–327. [[CrossRef](#)]

51. Xiong, X.; Geng, X.; Angal, A.; Sun, J.; Barnes, W. Using the Moon to track MODIS reflective solar bands calibration stability. *Sens. Syst. Next-Gener. Satell.* **XV** **2011**, 8176, 817611.
52. Wilson, T.; Xiong, X. Subsample difference correction for Terra MODIS SWIR bands 5–7 using lunar observations. *Sens. Syst. Next-Gener. Satell.* **XXII** **2018**, 10785, 107851B.
53. Sun, J.; Xiong, X.; Angal, A.; Chen, H.; Wu, A.; Geng, X. Time-Dependent Response Versus Scan Angle for MODIS Reflective Solar Bands. *IEEE Trans. Geosci. Remote Sens.* **2013**, *52*, 3159–3174. [[CrossRef](#)]
54. Moyer, D.; De Luccia, F.; Haas, E. JPSS-1 VIIRS reflective solar band on-orbit calibration performance impacts due to SWIR nonlinearity artifacts. *Sens. Syst. Next-Gener. Satell.* **XX** **2016**, 10000, 1000014.
55. Lei, N.; Xiong, X.; Guenther, B. Modeling the Detector Radiometric Gains of the Suomi NPP VIIRS Reflective Solar Bands. *IEEE Trans. Geosci. Remote Sens.* **2015**, *53*, 1565–1573. [[CrossRef](#)]
56. Kurucz, R.L. The solar irradiance by computation. In Proceedings of the 17th Annual Conference on Atmospheric Transmission Models, Bedford, MA, USA, 6–8 June 1995; Volume 95, pp. 333–334.
57. Xiong, X.; Cao, C.; Chander, G. An overview of sensor calibration inter-comparison and applications. *Front. Earth Sci. China* **2010**, *4*, 237–252. [[CrossRef](#)]
58. Moeller, C.; McIntire, J.; Schwarting, T.; Moyer, D. VIIRS F1 “best” relative spectral response characterization by the government team. *Earth Obs. Syst.* **XVI** **2011**, 8153, 81530K.
59. Moeller, C.; Schwarting, T.; McIntire, J.; Moyer, D.; Zeng, J. JPSS-1 VIIRS version 2 at-launch relative spectral response characterization and performance. *Earth Obs. Syst.* **XXI** **2016**, 9972, 997203.
60. Coddington, O.M.; Richard, E.C.; Harber, D.; Pilewskie, P.; Woods, T.N.; Chance, K.; Liu, X.; Sun, K. The TSIS-1 Hybrid Solar Reference Spectrum. *Geophys. Res. Lett.* **2021**, *48*, e2020GL091709. [[CrossRef](#)]
61. Sun, J.; Xiong, X. Improved Lunar Irradiance Model Using Multiyear MODIS Lunar Observations. *IEEE Trans. Geosci. Remote Sens.* **2021**, *59*, 5154–5170. [[CrossRef](#)]
62. Stone, T. Acquisition of Moon Measurements by Earth Orbiting Sensors for Lunar Calibration. *IEEE Trans. Geosci. Remote Sens.* **2022**, *60*, 1001706. [[CrossRef](#)]
63. Moyer, D.; Upreti, S.; Wang, W.; Cao, C.; Guch, I. S-NPP/NOAA-20 VIIRS reflective solar bands on-orbit calibration bias investigation. *Earth Obs. Syst.* **XXVI** **2021**, 11829, 1182912.
64. Xiong, X.; Angal, A.; Barnes, W.L.; Chen, H.; Chiang, V.; Geng, X.; Li, Y.; Twedt, K.; Wang, Z.; Wilson, T.; et al. Updates of Moderate Resolution Imaging Spectroradiometer on-orbit calibration uncertainty assessments. *J. Appl. Remote Sens.* **2018**, *12*, 034001. [[CrossRef](#)]
65. Lei, N.; Twedt, K.; McIntire, J.; Xiong, X. SNPP VIIRS RSB earth view reflectance uncertainty. In Proceedings of the 2017 IEEE International Geoscience and Remote Sensing Symposium (IGARSS), Fort Worth, TX, USA, 23–28 July 2017; pp. 5916–5919.
66. Wu, A.; Mu, Q.; Angal, A.; Xiong, X. Assessment of MODIS and VIIRS calibration consistency for reflective solar bands calibration using vicarious approaches. In Proceedings of the Sensors, Systems, and Next-Generation Satellites, XXIV, Online, 21–25 September 2020; Volume 11530, p. 1153018.
67. Upreti, S.; Cao, C.; Shao, X. Radiometric consistency between GOES-16 ABI and VIIRS on Suomi NPP and NOAA-20. *J. Appl. Remote Sens.* **2020**, *14*, 032407. [[CrossRef](#)]
68. Wang, W.; Cao, C. Evaluation of NOAA-20 VIIRS Reflective Solar Bands Early On-Orbit Performance Using Daily Deep Convective Clouds Recent Improvements. *IEEE J. Sel. Top. Appl. Earth Obs. Remote Sens.* **2020**, *13*, 3975–3985. [[CrossRef](#)]